Electromagnetic field of a moving charge in the presence of a left-handed medium

Sergey N. Galyamin* and Andrey V. Tyukhtin†
Physics Department, St. Petersburg State University, St. Petersburg, 198504, Russia
(Received 16 February 2010; revised manuscript received 5 May 2010; published 29 June 2010)

We analyze the electromagnetic field of a moving point charge in the presence of a "left-handed" medium (LHM). First, the case of uniform motion of the charge in infinite LHM was considered. Using complex function theory methods, we decomposed the total field into a "quasi-Coulomb" field, a wave field (Cherenkov radiation) and a "plasma trace." In addition, an effective numerical algorithm was developed for the total field computation, and typical plots were presented. It was shown that the wave field in LHM lags behind the charge more so than it does in ordinary medium. Furthermore, we investigated a charge intersecting the interface between vacuumlike medium and LHM. Asymptotic expressions for the field components were obtained and algorithms for their computation were developed. The spatial radiation can be separated into three distinct components, corresponding to ordinary transition radiation with a relatively large magnitude, Cherenkov radiation and reversed Cherenkov-transition radiation (RCTR). Rigorous conditions for generating RCTR were obtained: RCTR in the vacuum area was found to be the double threshold effect in both frequency and charge velocity domain. The RCTR decay in vacuum due to the losses in LHM was studied. Areas of the RCTR significance were determined and were found to be sufficiently large for observation. Possible applications to the beam diagnostics and the characterization of metamaterials were suggested.

DOI: 10.1103/PhysRevB.81.235134 PACS number(s): 41.60.Bq, 41.60.Dk, 41.20.−q

I. INTRODUCTION

Recent progress in design and fabrication of metamaterials (MTMs) allows the realization of a variety of electromagnetic properties not found in nature. MTM is, as a rule, a periodic structure comprising certain conductive, dielectric, or magnetic inclusions, with their size varying from hundreds of nanometers to millimeters. For an electromagnetic wave with a wavelength much larger than the unit-cell dimensions, the MTM is similar to a continuous medium and can be described by effective macroscopic parameters ε_{eff} and μ_{eff}. One attractive example of "metamedia" with exotic properties is that of "left-handed media" (LHM).

The idea of LHM, i.e., media simultaneously having negative permittivity ε and permeability μ, was introduced in the 1960s by Veselago.[1,2] Contrary to ordinary "right-handed" media (RHM), vectors $\vec{E}$, $\vec{H}$, and $\vec{k}$ form a left-handed orthogonal set in LHM. Therefore, the Poyting vector $\vec{S}=c/(4\pi)[\vec{E},\vec{H}]$ is opposite to the wave vector $\vec{k}$ and to the phase velocity. These peculiarities result in the unusual properties of wave processes in LHM.[1,2] In particular, an electromagnetic wave undergoes anomalous (negative) refraction at the RHM-LHM interface: the tangential projection of the Poyting vector of refracted wave is opposite to that of the incident wave.

Until recently no materials with negative μ have been found; therefore, LHM was merely a theoretical concept. At the same time, long before Veselago's papers,[1,2] certain questions concerning LHM were discussed indirectly by a number of researchers,[3–6] especially by Mandelshtam.[3,4] Mandelshtam has demonstrated that the essence of negative refraction is the "negative group velocity" effect, i.e., the opposite orientation of the group velocity (together with the energy flow $\vec{S}$) and the phase velocity.

Owing to the development of Pendry's ideas,[7,8] LHM were realized by means of MTMs.[9,10] The first real left-handed MTM was composed of double split-ring resonators and thin wires, producing negative μ_{eff} and negative ε_{eff}, respectively, in a common range of gigahertz (GHz) frequencies.[9,11] More recently MTMs with negative μ and negative refractive index at frequencies starting from THz up to the visible were demonstrated.[12–14] They use different unit cell designs, including, for example, single split-ring resonators, cut-wire pairs or "fishnet," depending on the operating frequency range.[15] Usually, the conductive elements are deposited at the dielectric substrate to get one monolayer of MTM. Distributing monolayers in an appropriate manner in the space, the three-dimensional structure can be built. It is remarkable that negative μ in natural medium (ferromagnetic metal) was also observed recently,[16] expanding the possibilities for the realization of LHM.

The "left-handed properties" can, in principle, be realized only inside a limited frequency range.[1,2] Therefore, it would be more correct to refer to a "left-handed frequency band" (LHFB) and a "right-handed frequency band" (RHFB) instead of LHM and RHM. However, as the term LHM is widely used in scientific literature, we will use it as well with the understanding that LHM is a medium possessing both LHFB and RHFB whereas RHM is a medium with RHFB only.

Starting from the first realization, different electromagnetic processes in LHM are actively investigated. Papers deal with the plane waves propagation in LHM and with their refraction at the RHM-LHM interface,[11,17–20] as well as with the extraction of the effective parameters ε_{eff} and μ_{eff} from scattering data.[21–23] Several papers are devoted to theoretical analysis of Cherenkov radiation (CR) in infinite or semi-infinite LHM (Refs. 24–26) (in particular, the effect of reversed CR was mentioned[24]) or to design and fabrication of the specific type of MTM suitable for the CR observation.[27] A recent experiment has proven the reversed nature of CR in LHM.[28] Transition radiation (TR) at the boundary with LHM was also partially analyzed.[29,30] Pafomov[29] appears to be the

first to mention the basic features of CR and TR at the frequency range with negative group velocity while Averkov[30] performed a more detailed analysis.

However, all papers devoted to CR and TR in the presence of LHM deal mainly with energetic characteristics of the far field while the field structure has practically not been studied. It is the main goal of this paper to investigate the field structure of both CR and TR in detail. We use approaches falling in the region of frequency domain technique. It should be noted that our earlier papers[31–37] were devoted to similar investigation of CR in the presence of different passive and active media.

II. ELECTROMAGNETIC FIELD OF THE MOVING POINT CHARGE IN INFINITE LHM

We consider the electromagnetic field of a point charge q uniformly moving in infinite (unbounded) LHM along the z axis in accordance with $z=Vt=c\beta t$. The charge density ρ_{q} and the current density $\vec{j}=j\vec{e}_z$ have the form

$$\rho_{\mathrm{q}} = q\,\delta(x)\,\delta(y)\,\delta(z-Vt), \quad j = V\rho_{\mathrm{q}}. \tag{1}$$

The medium is described by frequency-dependent permittivity $\varepsilon(\omega)$ and permeability $\mu(\omega)$ with nonzero losses: $\mathrm{Im}\,\varepsilon(\omega)>0$ and $\mathrm{Im}\,\mu(\omega)>0$ (for $\omega>0$). As LHM, the medium has both RHFB and LHFB:

$$\mathrm{RHFB:Re}\,\varepsilon(\omega)>0, \quad \mathrm{Re}\,\mu(\omega)>0,$$

$$\mathrm{LHFB:Re}\,\varepsilon(\omega)<0, \quad \mathrm{Re}\,\mu(\omega)<0. \tag{2}$$

A. Approach to the analysis of the integrals for the charge field components in an infinite medium

A convenient method for the investigation of such problems was developed in our previous papers.[35–38] This can be applied to the arbitrary frequency dispersion of $\varepsilon(\omega)$ and $\mu(\omega)$ but the resonant type of dispersion was investigated in more detail.[35,37] Fortunately, typical left-handed metamaterials usually possess this type of dispersion.[7–10] Consequently, our approach is well suited for this purpose. In the present section, we briefly summarize the main conditions of our method.

To distinguish the case of infinite medium from the case of RHM-LHM interface considered in Sec. III, we will mark the expressions for field components of a charge in infinite medium with the superscript "q." These expressions can be written in the cylindrical coordinate system ρ, φ, and z as follows:[39–41]

$$\begin{Bmatrix} E^{\mathrm{q}}_{\rho} \\ E^{\mathrm{q}}_{z} \\ H^{\mathrm{q}}_{\varphi} \end{Bmatrix} = \frac{q}{2c}\int_{-\infty}^{+\infty} d\omega \begin{Bmatrix} E^{\mathrm{q}}_{\rho\omega} \\ E^{\mathrm{q}}_{z\omega} \\ H^{\mathrm{q}}_{\varphi\omega} \end{Bmatrix} \exp\left(i\frac{\omega\zeta}{V}\right), \tag{3}$$

where

$$\begin{Bmatrix} E^{\mathrm{q}}_{\rho\omega} \\ E^{\mathrm{q}}_{z\omega} \\ H^{\mathrm{q}}_{\varphi\omega} \end{Bmatrix} = \begin{Bmatrix} is(\omega)[\beta\varepsilon(\omega)]^{-1}H^{(1)}_1[\rho s(\omega)] \\ -c\omega\varepsilon(\omega)^{-1}s^2(\omega)H^{(1)}_0[\rho s(\omega)] \\ is(\omega)H^{(1)}_1[\rho s(\omega)] \end{Bmatrix} \tag{4}$$

$\zeta=z-Vt$, $\beta=V/c$, $s^2=\omega^2V^{-2}[n^2(\omega)\beta^2-1]$, $n^2=\varepsilon\mu$, and $H^{(1)}_{0,1}$ are the Hankel functions, and function $s(\omega)$ is determined on the real axis ω in accordance with the absorption principle[42]

$$\mathrm{Im}\,s(\omega)>0. \tag{5}$$

This requirement means that the Fourier harmonics of charge's field components must decay exponentially with the increase in distance ρ. Further, the purpose is to calculate integrals in Eq. (3) in one way or another.

The essence of our approach is the following. We determine the function $s(\omega)$ in the entire complex plane ω in such a manner that Eq. (5) is fulfilled on the real axis. We draw the cuts in segments where $\mathrm{Im}\,s(\omega)=0$, fixing the "physical" sheet of the Riemann surface by the same condition (5). The following helpful properties then occur.[36,37]

If the integration path Γ consists of two parts, with one of them (Γ_+) lying in the domain $\mathrm{Re}\,\omega>0$ and the other (Γ_-) lying in the domain $\mathrm{Re}\,\omega<0$ with the total Γ being symmetrical with respect to the imaginary axis, then we get

$$\int_{\Gamma} F^{\mathrm{q}}_{\omega}\exp\left(\frac{i\omega\zeta}{V}\right)d\omega = 2\int_{\Gamma_+}\mathrm{Re}\left[F^{\mathrm{q}}_{\omega}\exp\left(\frac{i\omega\zeta}{V}\right)d\omega\right], \tag{6}$$

where F^{q}_{ω} is any of functions (4). Both the integration path in Eq. (3) and the ones to be used in further analysis possess the required symmetry. Thus, we can consider the domain $\mathrm{Re}\,\omega>0$ only. Next, the asymptote of the steepest-descent path (SDP) for integrands in Eq. (3) has importance for subsequent analysis. It is determined by the equation

$$\rho\sqrt{1-\beta^2}\,\mathrm{Im}\,\omega = \zeta|\mathrm{Re}\,\omega| + \mathrm{const}, \quad |\omega|\to\infty \tag{7}$$

(the value of const is unessential for us). Further manipulations are based on applying methods of complex function theory together with properties (6) and (7) to the calculation of integrals in Eq. (3).

B. Case of a left-handed medium

Here, we apply the above approach to the case of an LHM. We use the following typical model for the left-handed metamaterial:[7–10,30]

$$\varepsilon(\omega) = 1 - \frac{\omega^2_{\mathrm{pe}}}{\omega^2 + 2i\omega_{\mathrm{de}}\omega},$$

$$\mu(\omega) = 1 + \frac{\omega^2_{\mathrm{pm}}}{\omega^2_{\mathrm{rm}} - 2i\omega_{\mathrm{dm}}\omega - \omega^2}, \tag{8}$$

where ω is a frequency, ω_{pe} and ω_{pm} are, correspondingly, electric and magnetic "plasma" frequencies, ω_{rm} is a magnetic resonance frequency, and parameters ω_{de} and ω_{dm} are responsible for losses. It should be noted that ω^2_{pm} is usually replaced by $\alpha\omega^2$ ($0<\alpha<1$) but this is not important for the description of principal properties. Further analytical investigation is performed for the lossless medium ($\omega_{\mathrm{de}}=\omega_{\mathrm{dm}}$

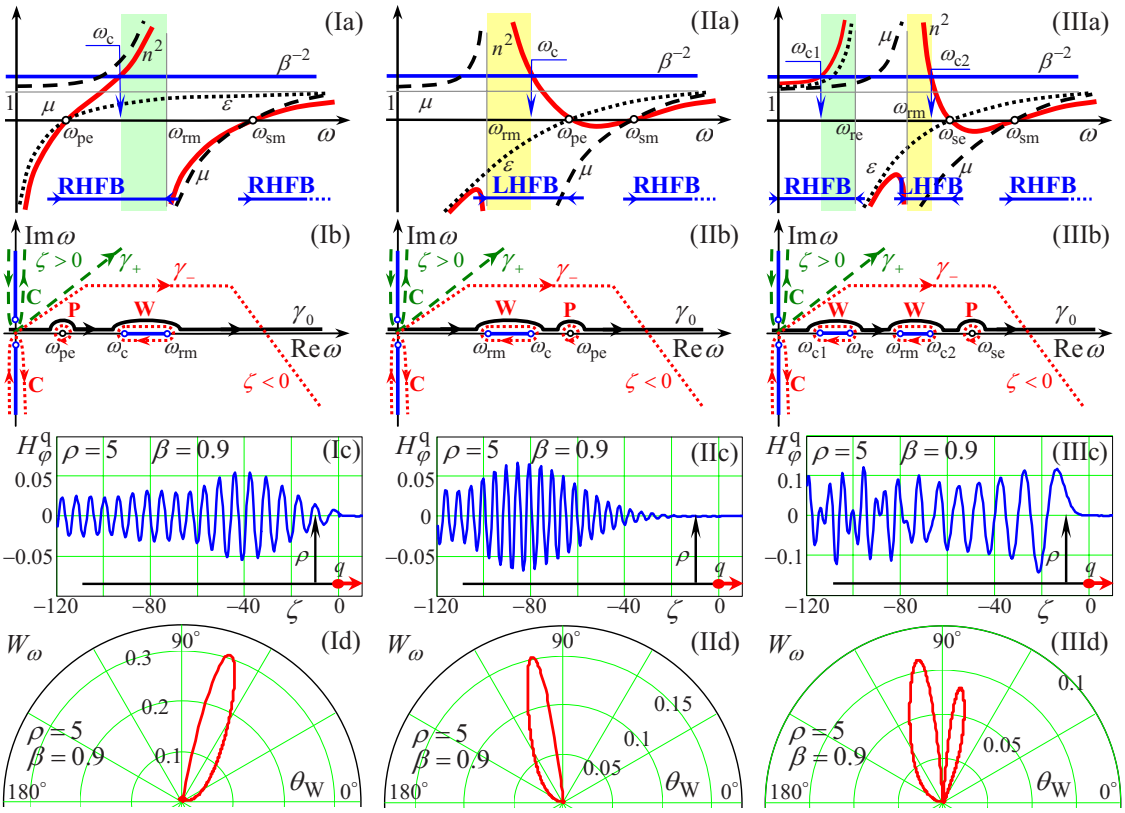

FIG. 1. (Color online) (a) Typical view of dispersion laws, (b) complex plane ω, (c) magnetic field plots, and (d) energy patterns for the case of (I) RHM, (II) LHM, and a (III) "mixed" medium (having the radiation frequency bands inside both RHFB and LHFB). For cases (I) and (II), the media are described by Eq. (8) with the following parameters (in units of ω_{rm}): (I)—$\omega_{pm}=1$ and $\omega_{pe}=0.6$; (II)—$\omega_{pm}=1$ and $\omega_{pe}=2$. Case (III) deals with both $\varepsilon(\omega)$ and $\mu(\omega)$ of resonant type: $\omega_{pm}=1$, $\omega_{pe}=1.7$, and $\omega_{re}=0.9$. In all cases, $\omega_{de}=\omega_{dm}=10^{-4}$. H_φ is in units $q\omega_{rm}^2c^{-2}$; W_ω is in units $q^2\omega_{rm}^3c^{-3}$; and ζ and ρ are in units $c\omega_{rm}^{-1}$.

$=0$) although a numerical algorithm can be used for arbitrary losses.

The frequency range of radiation is determined by the condition $s^2(\omega)>0$. If $\omega_{pe}<\omega_{rm}$, then the medium has two RHFBs ($\omega_{pe}<\omega<\omega_{rm}$ and $\omega>\omega_{sm}=\sqrt{\omega_{pm}^2+\omega_{rm}^2}$) with the radiation frequency range $\omega_c<\omega<\omega_{rm}$ lying in the first one [Fig. 1(Ia)]. In the case of $\omega_{pe}>\omega_{rm}$, the medium along with RHFB ($\omega>\omega_{sm}$) has an LHFB ($\omega_{rm}<\omega<\omega_{pe}$) containing the radiation frequency range $\omega_{rm}<\omega<\omega_c$ [Fig. 1(IIa)]. The parameter ω_c is determined by $s(\omega_c)=0$

$$\omega_c^2=\frac{a+[a^2+4\beta^2(1-\beta^2)\omega_{pe}^2(\omega_{rm}^2+\omega_{pm}^2)]^{1/2}}{2(1-\beta^2)},$$

$$a=\omega_{rm}^2(1-\beta^2)-(\omega_{pe}^2+\omega_{pm}^2).$$

Figures 1(Ib) and 1(IIb) shows the cuts [determined by equation $\mathrm{Im}\, s(\omega)=0$] and the integration path in the region $\mathrm{Re}\,\omega>0$ of complex plane ω [according to Eq. (6)]. It is important that the integration path γ_0 is located on the upper bank of cuts, where $\mathrm{sgn}\, s=\mathrm{sgn}\,\omega$ for RHM and $\mathrm{sgn}\, s=-\mathrm{sgn}\,\omega$ for LHM. Thus, the projection of the phase velocity in the radial direction $\vec{\rho}$ is positive for RHM and negative for LHM.

One of the possible analytical manipulations consists of the formation of the closed integration contour and the calculation of contributions of cuts and poles. The contours surrounding these singularities are shown in Figs. 1(Ib) and 1(IIb). As a result, we obtain

$$E_\rho^q=E_{\rho C}^q+E_{\rho W}^q+E_{\rho P}^q,\quad E_z^q=E_{zC}^q+E_{zW}^q+E_{zP}^q,\quad H_\varphi^q=H_{\varphi C}^q+H_{\varphi W}^q, \tag{9}$$

$$\begin{Bmatrix}E_{\rho C}^q\\E_{zC}^q\\H_{\varphi C}^q\end{Bmatrix}=\frac{q}{c}\int_0^\infty\begin{Bmatrix}s(i\tilde\omega)[\beta\varepsilon(i\tilde\omega)]^{-1}J_1(\rho|s(i\tilde\omega)|)\\\tilde\omega(1-n^2(i\tilde\omega)\beta^2)[c\beta^2\varepsilon(i\tilde\omega)]^{-1}J_0(\rho|s(i\tilde\omega)|)\mathrm{sgn}\,\zeta\\s(i\tilde\omega)J_1(\rho s(i\tilde\omega))\end{Bmatrix}\exp\left(-\tilde\omega\frac{|\zeta|}{V}\right)d\tilde\omega, \tag{10}$$

$$\begin{Bmatrix} E^{\mathrm{q}}_{\rho\mathrm{W}} \\ E^{\mathrm{q}}_{z\mathrm{W}} \\ H^{\mathrm{q}}_{\varphi\mathrm{W}} \end{Bmatrix} = -\frac{2q}{c}\int_{\min(\omega_{\mathrm{c}},\omega_{\mathrm{rm}})}^{\max(\omega_{\mathrm{c}},\omega_{\mathrm{rm}})} \begin{Bmatrix} s(\omega)[\beta\varepsilon(\omega)]^{-1}J_1[\rho s(\omega)]\sin(\omega\zeta V^{-1}) \\ \mu c^{-1}[1-n^{-2}(\omega)\beta^{-2}]\omega J_0[\rho s(\omega)]\cos(\omega\zeta V^{-1}) \\ s(\omega)J_1[\rho s(\omega)]\sin(\omega\zeta V^{-1}) \end{Bmatrix} d\omega\Theta(-\zeta), \tag{11}$$

$$\begin{Bmatrix} E^{\mathrm{q}}_{\rho\mathrm{P}} \\ E^{\mathrm{q}}_{z\mathrm{P}} \end{Bmatrix} = \frac{4q}{c^2\beta^2}\Theta(-\zeta)\frac{\omega}{d\varepsilon/d\omega} \begin{Bmatrix} K_1(\omega\rho V^{-1})\sin(\omega\zeta V^{-1}) \\ -K_0(\omega\rho V^{-1})\cos(\omega\zeta V^{-1}) \end{Bmatrix}\Bigg|_{\omega=\omega_{\mathrm{pe}}}, \tag{12}$$

where $J_m(\xi)$ and $K_m(\xi)$ are, respectively, the Bessel function and the modified Hankel function of m order, and $\Theta(\xi)$ is the Heaviside step function: $\Theta(\xi)=0$ at $\xi<0$, $\Theta(\xi)=1$ at $\xi>0$. Here, the index C is assigned to the "quasi-Coulomb" part of the field (contributions of cuts along the imaginary axis), the index W is assigned to the wave part (contributions of cuts along the real axis), and the index P is assigned to the so-called "plasma trace" (contributions of poles $\pm\omega_{\mathrm{pe}}$) [see Figs. 1(Ib) and 1(IIb)]. The quasi-Coulomb field exists both behind and in front of the moving charge and quickly decreases with distance from it. The wave field (CR) exists only behind the charge and oscillates with distance from it. Unlike the radiation field, the plasma trace is concentrated close to the charge movement trajectory and exponentially decreases with increasing ρ. Analogous expressions for a resonant RHM are given in our previous works.[35,37] The representation (9) has a clear physical meaning. Additionally, it possesses certain advantages for computing. One of them is that integrands in Eqs. (10) and (11) are free from Hankel functions, in contrast to the initial formula (4). Therefore, Eqs. (10) and (11) are convenient for computation of the wave and quasi-Coulomb fields for small values of ρ, including $\rho=0$.

Another possible method of investigation is based on certain transformation of the integration path.[35–37] For relatively small values of ω, it is convenient to transform contour γ_0 in such a way that it bypasses all branch points and poles. For the best convergence at large values of ω, we can use the contour parallel to the SDP asymptote [Eq. (7)]. Thus, for $\zeta>0$, we use the semi-infinite rays parallel to the SDP as the new integration path, while for $\zeta<0$, the trapezoidal contour with the half-infinite part parallel to the SDP asymptote is utilized [contours $\gamma_{\pm}$ in Figs. 1(Ib) and 1(IIb)]. This transformation allows the avoidance of the intersection of the integrands' singularities. The essential advantage of such an approach is the possibility of choosing the most convenient parameters of the new contour for the concrete parameters of the problem.

Some examples of computations of the H^{q}_{φ} component are shown in Figs. 1(Ic) and 1(IIc). Figures 1(Id) and 1(IId) also shows corresponding energetic patterns, defined by the following method.[24] The total energy passing through a unit square is equal to $W_{\rho}=\int_{-\infty}^{\infty}S_{\rho}dt$ (for a square parallel to the z axis) and $W_z=\int_{-\infty}^{\infty}S_z dt$ (for a square orthogonal to the z axis). These values can be represented as integrals from the spectral density of energy: $W_{\rho}=\int_0^{\infty}W_{\rho\omega}d\omega$ and $W_z=\int_0^{\infty}W_{z\omega}d\omega$. For $|s|\rho\gg 1$, the following approximations can be made:

$$W_{\rho\omega}\approx\frac{q^2}{2\pi\rho}\mathrm{Re}[|s|s(\omega\varepsilon)^{-1}\exp(-2\rho\ \mathrm{Im}\ s)],$$

$$W_{z\omega}\approx\frac{q^2}{2\pi V\rho}\mathrm{Re}[|s|\varepsilon^{-1}\ \exp(-2\rho\ \mathrm{Im}\ s)]. \tag{13}$$

The dependence of $W_{\omega}=\sqrt{W_{\rho\omega}^2+W_{z\omega}^2}$ on the angle $\theta_{\mathrm{W}}=\mathrm{atan}(W_{\rho\omega}/W_{z\omega})$ is the energetic pattern of radiation. Figures 1(Ic) and 1(Id) are related to the case of a medium only having radiation frequencies inside RHFB while Figs. 1(IIc) and 1(IId) are related to the case of a medium with a radiation band lying entirely inside LHFB. One can see that the pattern in the LHFB case is "reversed." Additionally, the increase in the field amplitude with $|\zeta|$ in LHM is slower compared with that in RHM. Obviously, this is due to the fact that the wave field in LHM lags behind the charge more so than it does in the RHM case.

Figures 1(IIIa)–(IIId) are related to a more complex case. Here, we use the model of resonant permeability [as in Eq. (8)] and resonant permittivity: $\varepsilon(\omega)=1+\omega_{\mathrm{pe}}^2(\omega_{\mathrm{re}}^2-2i\omega_{\mathrm{de}}\omega-\omega^2)^{-1}$. Parameters for Figs. 1(IIIa)–(IIId) are selected so that the medium has radiation frequency ranges inside both RHFB and LHFB. Therefore, the pattern has two lobes corresponding to ordinary and reversed CR [Figs. 1(IIId)]. On the magnetic field plot [Figs. 1(IIIc)], one can see that, for relatively small distance $|\zeta|<70$, the field is nearly sinusoidal; however, for $|\zeta|>70$, the field behavior is more complicated. This is explained by the addition of the left-handed CR for sufficiently large distances.

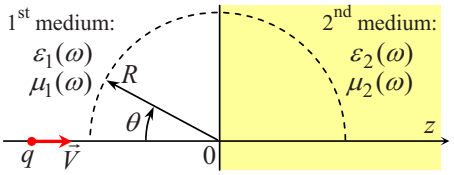

FIG. 2. (Color online) Geometry of the problem.

III. CASE OF A CHARGE CROSSING THE RHM-LHM INTERFACE

Here, we analyze the electromagnetic field generated by a charge q intersecting the interface (located at $z=0$) between two homogeneous isotropic frequency-dispersive media described by permittivity and permeability: $\varepsilon_1(\omega)$, $\mu_1(\omega)$ for $z<0$ and $\varepsilon_2(\omega)$, $\mu_2(\omega)$ for $z>0$ (Fig. 2). It is assumed that both media possess nonzero losses; i.e., small positive values

of Im $\varepsilon_{1,2}$ and Im $\mu_{1,2}$ (for $\omega>0$) are taken into account.

We suppose that the medium filling the region $z>0$ is LHM; i.e., it possesses both LHFB and RHFB [see Eq. (2)] while the volume $z<0$ is filled with RHM, i.e., a medium with RHFB only. The charge moves uniformly along the z axis in accordance with Eq. (1). The conditions of continuity of tangential components of electric ($\vec{E}$) and magnetic ($\vec{H}$) strengths must be satisfied in the plane $z=0$.

The electromagnetic field in the present geometry is presented as a sum of the "forced" field (superscript q) and the "free" field (superscript "b").[43,44] If index 1 refers to the area $z<0$ and index 2 refers to the area $z>0$, then

$$\begin{Bmatrix} E_\rho^{1,2} \\ E_z^{1,2} \\ H_\varphi^{1,2} \end{Bmatrix} = \begin{Bmatrix} E_\rho^{q1,2} \\ E_z^{q1,2} \\ H_\varphi^{q1,2} \end{Bmatrix} + \begin{Bmatrix} E_\rho^{b1,2} \\ E_z^{b1,2} \\ H_\varphi^{b1,2} \end{Bmatrix}. \tag{14}$$

The "forced" field ($E_\rho^{q1,2}$, $E_z^{q1,2}$, and $H_\varphi^{q1,2}$) as a charge field in the corresponding unbounded medium is described by formulas (3) and (4), and the analysis of the Sec. II is fully applicable to it. The free field arises due to the boundary (thus, it is marked by superscript b) and is described by the following formulas:[44]

$$\begin{Bmatrix} E_\rho^{b1,2} \\ E_z^{b1,2} \\ H_\varphi^{b1,2} \end{Bmatrix} = \frac{iq}{2\pi\beta}\int_{-\infty}^{\infty} d\omega \begin{Bmatrix} E_{\rho\omega}^{b1,2} \\ E_{z\omega}^{b1,2} \\ H_{\varphi\omega}^{b1,2} \end{Bmatrix} e^{-i\omega t}, \tag{15}$$

$$\begin{Bmatrix} E_{\rho\omega}^{b1,2} \\ E_{z\omega}^{b1,2} \\ H_{\varphi\omega}^{b1,2} \end{Bmatrix} = \int_{-\infty}^{\infty} dk_\rho \begin{Bmatrix} \dfrac{k_z^{(1,2)} H_1^{(1)}(\rho k_\rho)}{\mp \omega\varepsilon_{1,2}(\omega)} \\ \dfrac{ik_\rho H_0^{(1)}(\rho k_\rho)}{\omega\varepsilon_{1,2}(\omega)} \\ c^{-1} H_1^{(1)}(\rho k_\rho) \end{Bmatrix} B^{(1,2)} e^{ik_z^{(1,2)}|z|}, \tag{16}$$

$$B^{(1,2)}(k_\rho,\omega) = \frac{k_\rho^2}{g_3}\left(\frac{\beta\varepsilon_{1,2}k_z^{(1,2)} \mp \dfrac{\omega\varepsilon_{2,1}}{c}}{s_{1,2}^2 - k_\rho^2} - \frac{\beta^2\varepsilon_{2,1}}{\beta k_z^{(2,1)} \pm \dfrac{\omega}{c}} \right), \tag{17}$$

where $H_{0,1}^{(1)}(\xi)$ are the Hankel functions, $s_{1,2}(\omega) = \sqrt{\omega^2(\beta c)^{-2}(n_{1,2}^2\beta^2 - 1)}$, $k_z^{(1,2)}(k_\rho,\omega) = \sqrt{\omega^2 n_{1,2}^2 c^{-2} - k_\rho^2}$, $n_{1,2}^2(\omega) = \varepsilon_{1,2}(\omega)\mu_{1,2}(\omega)$, and $g_3(k_\rho,\omega) = \varepsilon_1 k_z^{(2)} + \varepsilon_2 k_z^{(1)}$. Each of functions $s_{1,2}$ is determined by Eq. (5) and functions $k_z^{(1,2)}$ are also determined (according to the absorption principle) by these rules

$$\operatorname{Im} k_z^{(1,2)} > 0. \tag{18}$$

Condition (18) means that the Fourier components of the free field must exponentially decay with increasing distance $|z|$. In the region $z<0$ (RHM), condition (18) results in Re $k_z^{(1)}>0$ for all frequencies. In the region $z>0$ (LHM), one obtains from condition (18) that Re $k_z^{(2)}>0$ for the RHFB but Re $k_z^{(2)}<0$ for the LHFB. The same results can be obtained for lossless media if the so-called Mandelshtam condition is used.[45]

It should be noted that a property similar to Eq. (6) can be obtained for the free field integrals in Eq. (15)

$$\int_\Gamma F_\omega^b \exp(-i\omega t)d\omega = 2\int_{\Gamma_+} \operatorname{Re}[F_\omega^b \exp(-i\omega t)d\omega], \tag{19}$$

where contour Γ is symmetrical with respect to the imaginary axis, Γ_+ is the part of Γ lying in the domain Re $\omega>0$, and F_ω^b is any of functions (16). It was found that the real axis ω is the convenient integration path for the calculation of Eq. (15). Thus, according to Eq. (19), it is sufficient to only consider positive frequencies: $\omega>0$.

Two methods are utilized for the analysis of the free field (15). The first is the asymptotic analytical approach based on the steepest-descent technique. An analogous technique was used for the RHM-RHM transition.[46–48] This is suitable to the analysis of the free-field Fourier harmonics (16). The second one is the numerical algorithm for computing both Fourier harmonics of the free field (16) and the total free field (15).

A. Analytical approach

Here, we obtain asymptotic expressions for the free-field Fourier harmonics (16) using the steepest-descent technique. Integrands in Eq. (16) contain four branch points $\pm\kappa_{1,2}$ ($\kappa_{1,2}=\omega c^{-1}n_{1,2}$, $n_{1,2}=\sqrt{n_{1,2}^2}$, and Im $n_{1,2}>0$), corresponding cuts (going along lines Im $k_z^{(1,2)}=0$) and three different types of poles: $\pm s_1$, $\pm s_2$, and the roots k_ρ^{P3} of equation $g_3(k_\rho)=0$.

Figures 3(Ia) and 3(IIa) demonstrate the typical view of complex plane k_ρ in two situations: the frequency under consideration is in RHFB (Ia) or in LHFB (IIa) (for the second medium). It is assumed that $|\operatorname{Re}\kappa_2|>\operatorname{Re}\kappa_1$. It is noteworthy that in the LHFB case, the branch points $\pm\kappa_2$ lie in the second and fourth quadrants, correspondingly, in contrast to the first and third quadrants in the RHFB case. In other words, Re $\kappa_2>0$ for RHFB and Re $\kappa_2<0$ for LHFB.

It is assumed that the Cherenkov condition is fulfilled at a given frequency in medium 2 (Re $s_2^2>0$). Therefore, poles $\pm s_2$ indicated in Figs. 3(Ia) and 3(IIa) are situated near the real axis. This is the case when their contributions are essential (otherwise, they are exponentially small). These poles describe the reflected and refracted CR in the LHFB case.[29,30] We call these waves the reversed Cherenkov-transition radiation (RCTR).[38]

It is also assumed that the Cherenkov condition in medium 1 is not fulfilled (Re $s_1^2<0$). Therefore, poles $\pm s_1$ give a quasi-Coulomb field, which is of no interest to us here (these poles are not indicated in Fig. 3). Furthermore, we restrict ourselves to investigation of only spherical and cylindrical waves (decreasing with distance as R^{-1} and $\rho^{-1/2}$). Because the pole k_ρ^{P3} describes the surface waves,[44] it is outside of our consideration (this pole is also not indicated in Fig. 3).

We will consider in detail the region $z<0$ and neglect losses in this area (supposing $n_1>0$). For convenience of

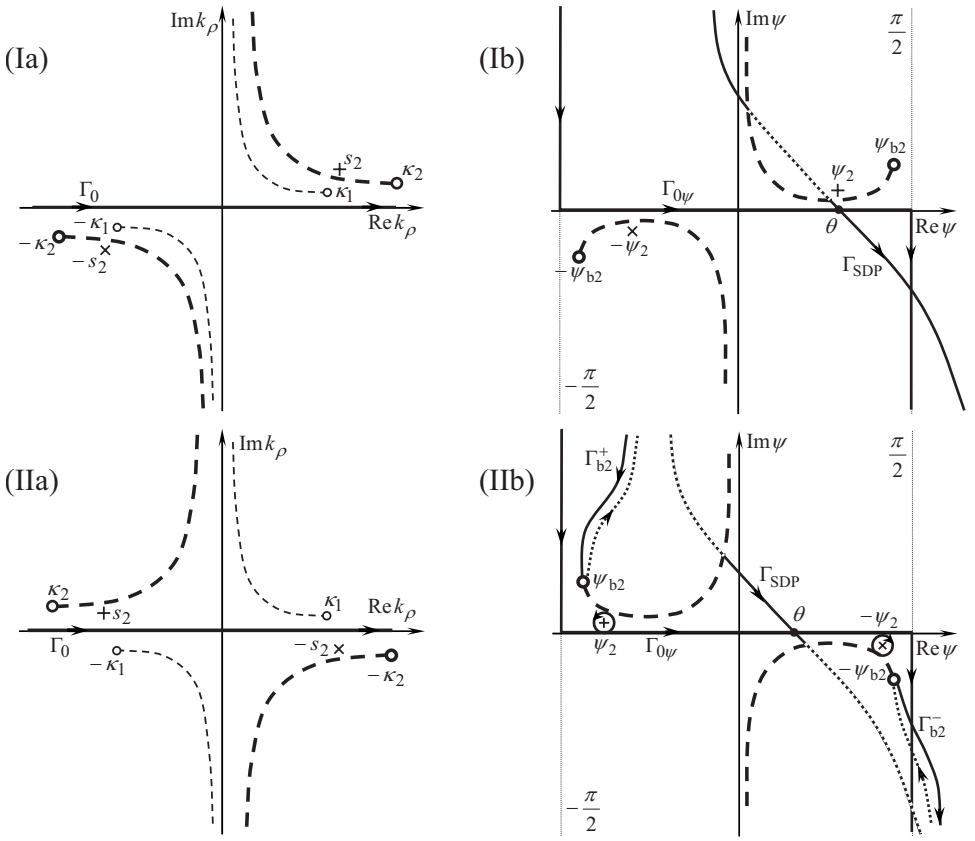

FIG. 3. Typical view of (a) complex plane k_ρ and (b) complex plane ψ for the situation where the frequency under consideration is in RHFB for the second medium (I) or in LHFB (II); $|\mathrm{Re}\,\kappa_2| > \mathrm{Re}\,\kappa_1$. Pictures (Ib) and (IIb) are related to the area $z<0$. The sign $\circ$ corresponds to the branch point, dashed lines correspond to cuts, signs + and $\times$ correspond to poles. Initial integration path in k_ρ plane Γ_0 corresponds to $\Gamma_{0\psi}$ in ψ plane. The dashed parts of contours lie in the Riemann's surface sheet with $\mathrm{Im}\,k_z^{(2)}<0$. Cherenkov condition is fulfilled in medium 2 only.

handling integrals in Eq. (16) with the steepest-descent technique, we introduce new spatial variables R and θ (Fig. 2) and a new complex variable ψ, where $k_\rho=\kappa_1 \sin\psi$ and $k_z^{(1)}=\kappa_1\cos\psi$.[49]

A typical view of the complex plane ψ for the RHFB situation is presented in Fig. 3(Ib) while the LHFB situation is shown in Fig. 3(IIb). Contour $\Gamma_{0\psi}$ corresponds to the initial integration path Γ_0 in k_ρ plane. Poles $\pm s_2$ are converted into $\pm\psi_2$ ($\sin\psi_2=\kappa_1^{-1}s_2$) and branch points $\pm\kappa_1$ disappear while $\pm\kappa_2$ are transformed into $\pm\psi_{\rm b2}$ ($\sin\psi_{\rm b2}=\kappa_1^{-1}\kappa_2$). Utilizing the aforementioned substitutions, we present Eq. (16) in the following form:

$$\begin{Bmatrix} E^{\rm b1}_{\rho\omega} \\ E^{\rm b1}_{z\omega} \\ H^{\rm b1}_{\varphi\omega} \end{Bmatrix} = \int_{\Gamma_{0\psi}} \begin{Bmatrix} e^{\rm b1}_{\rho\omega} H^{(1)}_1(R\kappa_1 \sin\theta\sin\psi) \\ e^{\rm b1}_{z\omega} H^{(1)}_0(R\kappa_1 \sin\theta\sin\psi) \\ h^{\rm b1}_{\varphi\omega} H^{(1)}_1(R\kappa_1 \sin\theta\sin\psi) \end{Bmatrix} \times \exp(iR\kappa_1\cos\theta\cos\psi)d\psi, \quad (20)$$

where

$$\begin{Bmatrix} e^{\rm b1}_{\rho\omega}(\psi,\omega) \\ e^{\rm b1}_{z\omega}(\psi,\omega) \\ h^{\rm b1}_{\varphi\omega}(\psi,\omega) \end{Bmatrix} = \begin{Bmatrix} \dfrac{\kappa_1^2(\cos\psi)^2}{\mp\omega\varepsilon_1} \\ \dfrac{i\kappa_1^2\sin(2\psi)}{2\omega\varepsilon_1} \\ c^{-1}\kappa_1\cos\psi \end{Bmatrix} B^{(1)}(\kappa_1\sin\psi,\omega). \quad (21)$$

Furthermore, using the asymptotic representation of the Hankel functions at $R|\kappa_1|\sin\theta\sin\psi \gg 1$, one can present Eq. (20) in the following convenient form:

$$\begin{Bmatrix} E^{\rm b1}_{\rho\omega} \\ E^{\rm b1}_{z\omega} \\ H^{\rm b1}_{\varphi\omega} \end{Bmatrix} \approx \int_{\Gamma_{0\psi}} \begin{Bmatrix} e^{\rm b1}_{\rho\omega}(\psi,\omega)e^{-3\pi i/4} \\ e^{\rm b1}_{z\omega}(\psi,\omega)e^{-\pi i/4} \\ h^{\rm b1}_{\varphi\omega}(\psi,\omega)e^{-3\pi i/4} \end{Bmatrix} \times \sqrt{\frac{2}{\pi R\kappa_1\sin\theta\sin\psi}}\exp[\Omega_1\phi_1(\psi)]d\psi, \quad (22)$$

where $\Omega_1=|\kappa_1|R$ and $\phi_1(\psi)=i\cos(\psi-\theta)$. The SDP passes through the saddle point $\psi_{S1}=\theta$ and satisfies the requirements $\mathrm{Im}\,\phi_1(\psi)=\mathrm{Im}\,\phi_1(\theta)$ and $\mathrm{Re}\,\phi_1(\psi)-\mathrm{Re}\,\phi_1(\theta)<0$. This SDP, marked as $\Gamma_{\rm SDP}$, is presented in Figs. 3(Ib) and 3(IIb). If $R|\kappa_1|\sin\theta\sin\psi\sim 1$, contour $\Gamma_{\rm SDP}$ is not a real SDP and is void of common benefits of SDP. However, we will use it in our manipulations.

In the RHFB case (index r), the transformation $\Gamma_{0\psi}\to\Gamma_{\rm SDP}$ leads to

$$\begin{Bmatrix} E^{\rm b1r}_{\rho\omega} \\ E^{\rm b1r}_{z\omega} \\ H^{\rm b1r}_{\varphi\omega} \end{Bmatrix} \approx \begin{Bmatrix} E^{\rm b1S}_{\rho\omega} \\ E^{\rm b1S}_{z\omega} \\ H^{\rm b1S}_{\varphi\omega} \end{Bmatrix}, \quad (23)$$

where

$$\begin{Bmatrix} E^{\rm b1S}_{\rho\omega} \\ E^{\rm b1S}_{z\omega} \\ H^{\rm b1S}_{\varphi\omega} \end{Bmatrix} = \int_{\Gamma_{\rm SDP}} \begin{Bmatrix} e^{\rm b1}_{\rho\omega} H^{(1)}_1(R\kappa_1 \sin\theta\sin\psi) \\ e^{\rm b1}_{z\omega} H^{(1)}_0(R\kappa_1 \sin\theta\sin\psi) \\ h^{\rm b1}_{\varphi\omega} H^{(1)}_1(R\kappa_1 \sin\theta\sin\psi) \end{Bmatrix} \times \exp(iR\kappa_1\cos\theta\cos\psi)d\psi. \quad (24)$$

In the LHFB situation (index ℓ), the transformation of $\Gamma_{0\psi}$ to

Γ_{SDP} is accompanied by the intersection of poles $\pm\psi_2$ [Fig. 3(IIb)]; thus

$$\begin{Bmatrix} E_{\rho\omega}^{\mathrm{b1}\ell} \\ E_{z\omega}^{\mathrm{b1}\ell} \\ H_{\varphi\omega}^{\mathrm{b1}\ell} \end{Bmatrix} \approx \begin{Bmatrix} E_{\rho\omega}^{\mathrm{b1S}} \\ E_{z\omega}^{\mathrm{b1S}} \\ H_{\varphi\omega}^{\mathrm{b1S}} \end{Bmatrix} + \begin{Bmatrix} E_{\rho\omega}^{\mathrm{b1P}} \\ E_{z\omega}^{\mathrm{b1P}} \\ H_{\varphi\omega}^{\mathrm{b1P}} \end{Bmatrix}, \tag{25}$$

where

$$\begin{Bmatrix} E_{\rho\omega}^{\mathrm{b1P}} \\ E_{z\omega}^{\mathrm{b1P}} \\ H_{\varphi\omega}^{\mathrm{b1P}} \end{Bmatrix} = 2\pi i \begin{Bmatrix} E_{\rho\omega}^{\mathrm{b1P+}} - E_{\rho\omega}^{\mathrm{b1P-}} \cdot \Theta(\theta_1^* - \theta) \\ E_{z\omega}^{\mathrm{b1P+}} - E_{z\omega}^{\mathrm{b1P-}} \cdot \Theta(\theta_1^* - \theta) \\ H_{\varphi\omega}^{\mathrm{b1P+}} - H_{\varphi\omega}^{\mathrm{b1P-}} \cdot \Theta(\theta_1^* - \theta) \end{Bmatrix}, \tag{26}$$

$$\begin{Bmatrix} E_{\rho\omega}^{\mathrm{b1P}\pm} \\ E_{z\omega}^{\mathrm{b1P}\pm} \\ H_{\varphi\omega}^{\mathrm{b1P}\pm} \end{Bmatrix} = \frac{\varepsilon_1}{n_1} \begin{Bmatrix} \dfrac{\pm \kappa_1 s_2 k_z^1(s_2) H_1^{(1)}(\pm s_2 R \sin\theta)}{\omega \varepsilon_1 g_3^*(\omega)} \\ \dfrac{-i\kappa_1 s_2^2 H_0^{(1)}(\pm s_2 R \sin\theta)}{\omega \varepsilon_1 g_3^*(\omega)} \\ \dfrac{\mp \kappa_1 s_2 H_1^{(1)}(\pm s_2 R \sin\theta)}{c g_3^*(\omega)} \end{Bmatrix} \times \exp[i k_z^{(1)}(s_2) R \cos\theta], \tag{27}$$

$$\theta_1^* = \theta_{10}^* - \delta\theta_1^*,$$

$$\theta_{10}^* = \operatorname{atan} \sqrt{\frac{\mathrm{Re}\, n_2^2\beta^2 - 1}{n_1^2\beta^2 - \mathrm{Re}\, n_2^2\beta^2 + 1}}, \quad \delta\theta_1^* = \sqrt{\frac{2}{R_1^*\kappa_1}}, \tag{28}$$

$$R_1^* = \frac{8(n_1^2\beta^2 - \mathrm{Re}\, n_2^2\beta^2 + 1)(\mathrm{Re}\, n_2^2\beta^2 - 1)}{\kappa_1 \beta^4 (\mathrm{Im}\, n_2^2)^2}, \tag{29}$$

$$g_3^*(\omega) = -\frac{\omega\varepsilon_1}{c\beta} + \varepsilon_2 k_z^{(1)}(s_2) \tag{30}$$

and $\Theta(\xi)$ is the Heaviside step function. Note that $\delta\theta_1^* \ll \theta_{10}^*$ because $R_1^*\kappa_1 \gg 1$ (see Appendix).

Note that integrals along SDPs $\Gamma_{\mathrm{b2}}^{\pm}$ originated from the corresponding branch points [Fig. 3(IIb)] have been excluded from asymptotic representation (25). This was made due to the fact that contributions of these paths represent lateral waves[49] and that their decrease with distance $\sim(R\sqrt{\rho})^{-1}$ is faster than that for spherical and cylindrical waves. Because only spherical and cylindrical waves are taken into account in our consideration, lateral waves have been neglected. Similar integrals arise in the RHFB case at certain conditions ($\mathrm{Re}\,\psi_{\mathrm{b2}} < \theta$) and they have been excluded from Eq. (23) on the same grounds.

The second term in Eq. (25) represents the RCTR in medium 1 being the transmitted Cherenkov radiation (it can be shown that this term matches at the boundary with the CR in medium 2). It only exists in the LHFB case. We call this part of field the RCTR for two reasons. First, this radiation possesses certain features of both Cherenkov and transition radiation. Similarly to TR, RCTR exists if there is a boundary, and similarly to CR, it arises when the Cherenkov condition is fulfilled. Second, we call this radiation "reversed" to underline that it stems from the reversed nature of CR in LHM.[38]

It is noteworthy that the poles' contribution (26) is essential in medium 1 only for $\mathrm{Re}[k_z^{(1)}(\pm s_2)]^2 > 0$; otherwise it is small due to the exponential term in Eq. (27). One can arrive to the following condition for the presence of RCTR in the area $z<0$:

$$\beta_{\mathrm{CR}}(\omega) < \beta < \beta_{\mathrm{TIR}}(\omega),$$

$$\beta_{\mathrm{CR}} = \frac{1}{|\mathrm{Re}\, n_2(\omega)|}, \quad \beta_{\mathrm{TIR}} = \frac{1}{\sqrt{\mathrm{Re}\, n_2^2(\omega) - n_1^2(\omega)}}. \tag{31}$$

The lower threshold of RCTR is the Cherenkov threshold for medium 2. The upper threshold is explained by the total internal reflection of CR and is only essential for $\mathrm{Re}\, n_2^2 > 1 + n_1^2$ (otherwise $\beta_{\mathrm{TIR}} > 1$).

It should be noted that Averkov[30] has also considered a charge crossing the vacuum-LHM interface and obtained a θ-dependent condition for the existence of transmitted CR in the area $z<0$. This is because the contribution of pole $-\psi_2$ is only taken into account in Averkov's paper.[30] However, as was demonstrated above, the pole ψ_2 contributes to the refracted CR at an arbitrary observation angle θ. Thus, condition (31) is not related to angle θ (it is θ-independent). Despite of this qualitative error, Averkov[30] gives the correct physical interpretation of the RCTR effect (see Sec. III B).

If the condition $R|\kappa_1|\sin\theta \sin\psi \gg 1$ is fulfilled, the contour Γ_{SDP} is the real SDP. Provided that $\Omega_1 \gg 1$, integral in Eq. (24) is practically determined by the small neighborhood of the saddle point $\psi_{\mathrm{S1}} = \theta$. As one can see from Fig. 3(Ib), the saddle point is isolated in the RHFB case (there are no poles in the vicinity of ψ_{S1}); thus, we obtain

$$\begin{Bmatrix} E_{\rho\omega}^{\mathrm{b1S}} \\ E_{z\omega}^{\mathrm{b1S}} \\ H_{\varphi\omega}^{\mathrm{b1S}} \end{Bmatrix} \approx \frac{\sqrt{2}h_1}{\sqrt{|\kappa_1|\sin\theta}} \begin{Bmatrix} e_{\rho\omega}^{\mathrm{b1}}(\theta,\omega) \\ e_{z\omega}^{\mathrm{b1}}(\theta,\omega) \\ h_{\varphi\omega}^{\mathrm{b1}}(\theta,\omega) \end{Bmatrix} \frac{\exp(i\kappa_1 R)}{R}, \tag{32}$$

where $h_1 = \sqrt{-2/\phi_1''(\theta)}$, $\arg h_1 = \arg(d\psi)|_{\psi=\theta}$, and $d\psi$ denotes an element along Γ_{SDP}. Expression (32) is valid at angles $1/\sqrt{\Omega_1} \ll \theta < \pi/2$ and represents the spherical wave of TR.

In the LHFB case, if condition (31) is fulfilled, the pole $-\psi_2$ may be near the saddle point θ [Fig. 3(IIb)] In this case, we have obtained the uniform asymptotic approximation (A1) for the integral in Eq. (24) valid for $\Omega_1 \gg 1$, $1/\sqrt{\Omega_1} \ll \theta < \pi/2$ regardless of the distance between the saddle point and the pole [i.e., Eq. (A1) is valid uniformly as $-\psi_2 \to \psi_{\mathrm{S1}} = \theta$].

In general, the asymptotic (A1) is more complicated as compared with Eq. (32) (not a simple spherical wave) and cannot be separated from the contribution of pole $-\psi_2$ due to the discontinuity at $\theta = \theta_1^*$. This discontinuity is exactly compensated by the contribution of pole $-\psi_2$.

However, when the distance between the saddle point and the pole is sufficiently large, the uniform asymptotic (A1) is greatly simplified. The rigorous consideration (see Appendix) gives the following result.

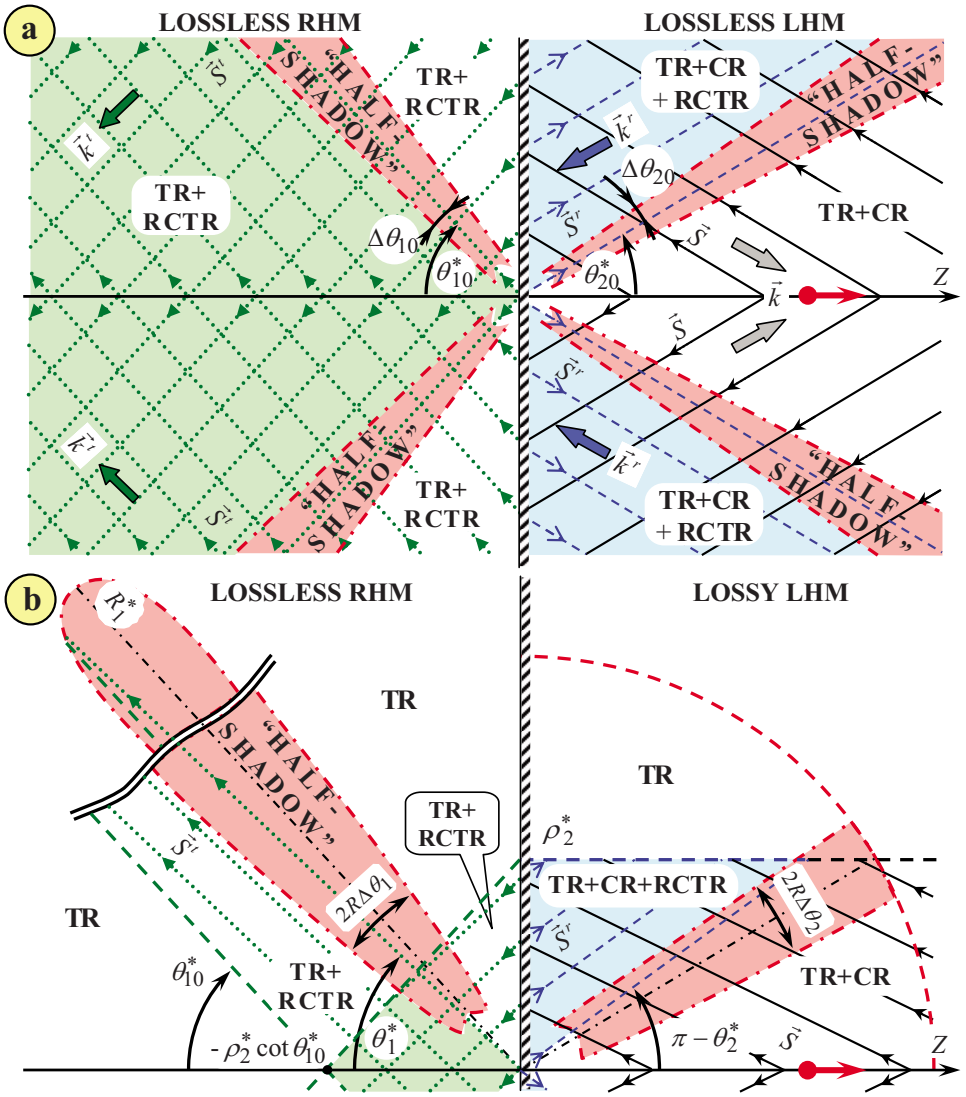

FIG. 4. (Color online) Areas of significance of the different parts of the electromagnetic field in the case of (a) lossless half-space $z>0$ and (b) lossy one (the half-space $z<0$ is lossless in both cases). The solid, dashed, and dotted lines are parallel to the Poyting vector of the reversed CR ($\vec{S}$), reflected RCTR ($\vec{S}'$), and transmitted RCTR ($\vec{S}''$), respectively. Lossless case (a): RCTR exists in the whole half-space $z<0$ (transmitted RCTR) and at angles $\pi/2<\theta<\pi-\theta^*_{20}$ in the half-space $z>0$ (reflected RCTR). Transmitted RCTR interfere at angles $0<\theta<\theta^*_{10}$, where dotted lines intersect each other. Reflected RCTR interfere with the reversed CR at angles $\pi/2<\theta<\pi-\theta^*_{20}$, where solid lines intersect dashed ones. Lossy case (b): transmitted RCTR exist inside the limited region hatched by the dotted lines. The maximum size of this region is determined by R^*_1. Both reversed CR and reflected RCTR exist inside the bounded region $\rho\lesssim\rho^*_1$. In both cases dash-dotted lines indicate boundaries of half-shadow areas: TR is a spherical wave outside these areas only. Half-shadow areas exist at arbitrary large R in the lossless case (a) and are limited in the lossy one (b). Typical values of parameter R^*_1 are presented in Fig. 5.

If losses in medium 2 are taken into account, one should use the asymptotic representation (A1) at $R\lesssim R^*_1$ within the angular interval $|\theta-\theta^*_1|\lesssim\Delta\theta_1$, where $\Delta\theta_1=\sqrt{2\Omega_1^{-1}(1-R/R^*_1)}$ [this area marked as "half-shadow" is indicated in Fig. 4(b)] As one can see, $\Delta\theta_1=0$ at $R=R^*_1$. However, outside the half-shadow area, one obtains

$$\begin{Bmatrix} E^{\mathrm{b1}\ell}_{\rho\omega} \\ E^{\mathrm{b1}\ell}_{z\omega} \\ H^{\mathrm{b1}\ell}_{\varphi\omega} \end{Bmatrix} \approx \begin{Bmatrix} E^{\mathrm{b1S}}_{\rho\omega} \\ E^{\mathrm{b1S}}_{z\omega} \\ H^{\mathrm{b1S}}_{\varphi\omega} \end{Bmatrix} + \begin{Bmatrix} E^{\mathrm{b1P}}_{R\omega} \\ E^{\mathrm{b1P}}_{z\omega} \\ H^{\mathrm{b1P}}_{\varphi\omega} \end{Bmatrix},$$

$$R\lesssim R^*_1, \quad 1/\sqrt{\Omega_1}\ll\theta<\pi/2, \quad |\theta-\theta^*_1|\gg|\Delta\theta_1|, \quad (33)$$

where the first term is given by Eq. (32) while the second one is given by Eq. (26). As one can see, TR (the saddle-point contribution) is a spherical wave in this case and can be considered separately from the RCTR (cylindrical waves). Analyzing the second term in Eq. (33) (RCTR) one can obtain that RCTR in the lossless area $z<0$ diminish exponentially [see Eq. (A6)]. The least decay is exhibited by the contribution of pole $-\psi_2$ at $\theta=\theta^*_1$

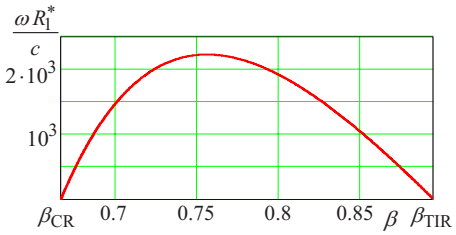

FIG. 5. (Color online) Dependence of $\omega c^{-1}R_1^*$ (see Fig. 4) on the charge velocity β. Media parameters are $n_1=1$, $n_2=-1.5+i0.01$, $\beta_{CR}=0.67$, and $\beta_{TIR}=0.89$.

$$\begin{Bmatrix} |E_{\rho\omega}^{b1P-}| \\ |E_{z\omega}^{b1P-}| \\ |H_{\varphi\omega}^{b1P-}| \end{Bmatrix} \sim \exp\left(-\frac{2R}{R_1^*}\right), \quad \theta = \theta_1^*. \tag{34}$$

As a result, RCTR is essential inside the limited area only [the region hatched by the dotted lines in Fig. 4(b)]. Outside this area contribution of the poles is diminished at least by the factor of e^2.

If $R \gg R_1^*$, the contribution of the poles is negligible [see Eq.(A6) and Fig. 4(b)]; thus

$$\begin{Bmatrix} E_{\rho\omega}^{b1\ell} \\ E_{z\omega}^{b1\ell} \\ H_{\varphi\omega}^{b1\ell} \end{Bmatrix} \approx \begin{Bmatrix} E_{\rho\omega}^{b1S} \\ E_{z\omega}^{b1S} \\ H_{\varphi\omega}^{b1S} \end{Bmatrix}, \quad 1/\sqrt{\Omega_1} \ll \theta < \pi/2, \tag{35}$$

where $E_{\rho\omega}^{b1S}$, $E_{z\omega}^{b1S}$, and $H_{\varphi\omega}^{b1S}$ are given by Eq. (32). In this case, only spherical wave of TR is essential. Consequently, for the lossy half-space $z>0$ and the lossless half-space $z<0$, the parameter R_1^* determines the distance upon which both the uniform asymptotic (A1) and the contribution of the poles (RCTR) are of significance [of course, both asymptotic (A1) and RCTR (26) are essential inside the corresponding limited regions, Fig. 4(b)].

If losses in medium 2 are neglected, then $R_1^* \to \infty$, $\Delta\theta_1 \to \Delta\theta_{10}=\sqrt{2}\Omega_1^{-1/2}$, $\theta_1^*=\theta_{10}^*$, and uniform asymptotic (A1) is essential at arbitrarily large R inside the angular interval $|\theta - \theta_{10}^*| \lesssim \Delta\theta_{10}$ or inside the corresponding segment of a circle $2R\Delta\theta_{10}=2\sqrt{2R|\kappa_1|^{-1}}$ [half-shadow area in Fig. 4(a)]. Again, outside the half-shadow TR is a spherical wave. RCTR (26)

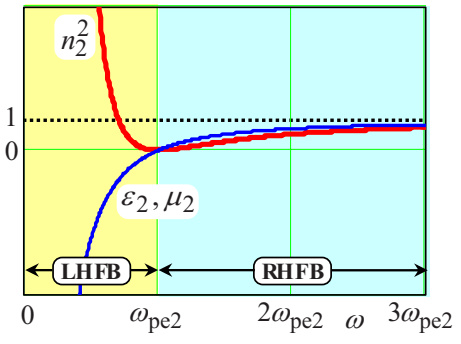

FIG. 6. (Color online) Dependencies of n_2^2 and $\varepsilon_2=\mu_2$ on frequency ω in the lossless case ($\omega_{de2}=\omega_{dm2}=0$). Medium 2 possesses both RHFB ($\omega>\omega_{pe2}$) and LHFB ($0<\omega<\omega_{pe2}$).

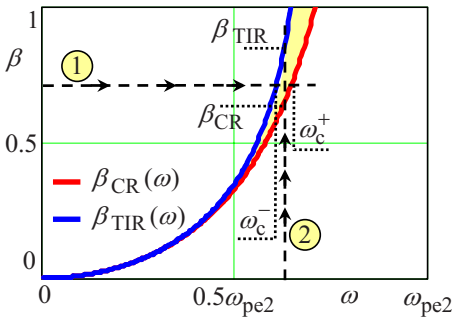

FIG. 7. (Color online) Dependence of the lower (β_{CR}) and upper (β_{TIR}) thresholds of the RCTR effect in vacuum on frequency. Allowable parameters (β, ω) of the RCTR effect in vacuum are those enclosed between β_{CR} and β_{TIR}. Dashed lines 1 and 2 are paths chosen for the demonstration (see Fig. 8).

is also essential at arbitrarily large R [Fig. 4(a)], and Eq. (33) is valid for $1/\sqrt{\Omega_1} \ll \theta < \pi/2$ and $|\theta - \theta_{10}^*| \gg \Delta\theta_{10}$.

An asymptotic approximation [similar to Eq. (A1)] correctly describing the field in medium 2 (for angles $\theta > \pi/2$ and $\pi - \theta \gg 1/\sqrt{R|\kappa_2|}$) can be similarly obtained. In particular, one can show that RCTR in medium 2 is connected with the contribution of the pole s_2 being the CR reflected from the boundary. If the Cherenkov condition is fulfilled ($\beta > \beta_{CR}$), this contribution exists at angles $\pi/2 < \theta < \theta_2^*$, where

$$\theta_2^* = \pi - (\theta_{20}^* + \delta\theta_2^*),$$

$$\theta_{20}^* = \operatorname{atan}\sqrt{\operatorname{Re} n_2^2\beta^2 - 1}, \quad \delta\theta_2^* = \sqrt{\frac{2}{R_2^*|\operatorname{Re}\kappa_2|}}, \tag{36}$$

$$R_2^* = \frac{8(\operatorname{Re} n_2^2)^2(\operatorname{Re} n_2^2\beta^2 - 1)}{|\operatorname{Re}\kappa_2|(\operatorname{Im} n_2^2)^2}, \quad R_2^*|\operatorname{Re}\kappa_2| \gg 1. \tag{37}$$

It should be noted that this pole may be near the saddle point in both RHFB and LHFB cases. Due to the losses the reversed CR ("forced" field) and the reflected RCTR (contribution of pole s_2) are significant for $\rho \lesssim \rho_2^*$ only, where $\rho_2^* = 4(\omega\beta|\operatorname{Im} n_2^2|)^{-1}\sqrt{\operatorname{Re} n_2^2\beta^2 - 1}$. For $\rho > \rho_2^*$ both CR and RCTR are diminished at least by the factor of e^2. TR is a spherical wave outside the half-shadow area: $|\theta - \theta_2^*| \gg \Delta\theta_2$, where $\Delta\theta_2 = \sqrt{2(R|\operatorname{Re}\kappa_2|)^{-1}(1 - R/R_2^*)}$ (Fig. 4). This spherical wave is essential at $R \lesssim \rho_2^*(\sin\theta_{20}^*)^{-1}$. The passage to the limit of negligible losses is analogous to that in medium 1.

To summarize the result of this section, one should mention the following points. The above analytical approach predicts the RCTR effect and gives rigorous mathematical conditions for it's presence: the double threshold condition (31) for medium 1 and condition $\beta > \beta_{CR}$, $\pi/2 < \theta < \theta_2^*$ for medium 2. As was shown, RCTR is connected with the contribution of poles. Areas of the RCTR significance were investigated in the case of lossless (vacuumlike) half-space $z<0$. In the case of lossy LHM [Fig. 4(b)] both reflected RCTR and CR are essential inside the cylinder $\rho \lesssim \rho_2^*$ only. Moreover, RCTR in the vacuumlike area possesses a weak exponential decay [see Eq. (A6)]. As a result, refracted RCTR is significant inside the limited region only [Fig. 4(b)]. It

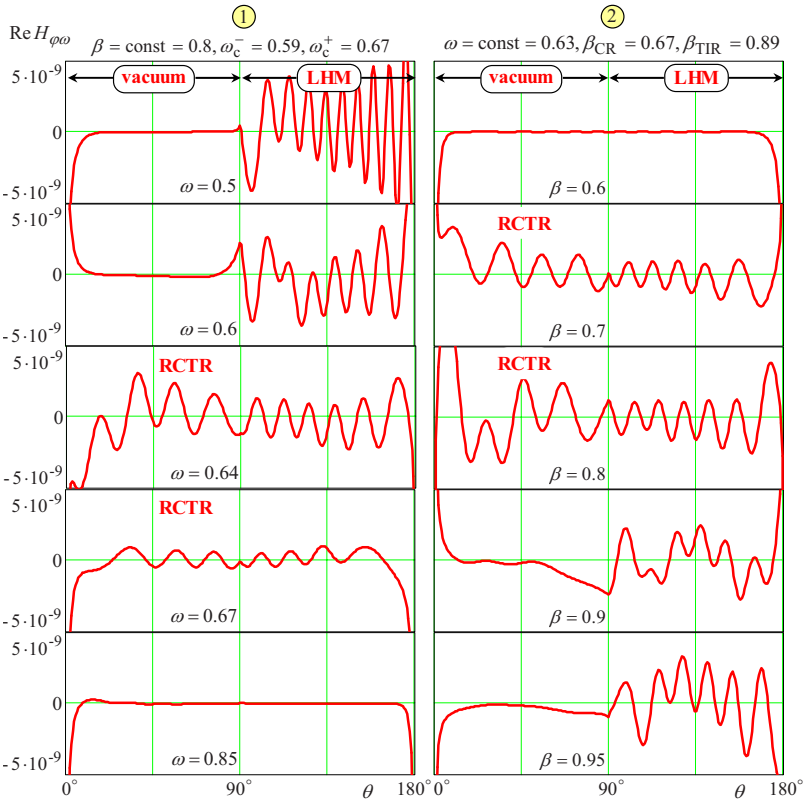

FIG. 8. (Color online) Modification of the spatial distribution of the magnetic field Fourier harmonic Re $H_{\varphi\omega}(\theta)$ (Vm^{-1} s) with increasing ω at constant β (1) and with increasing β at constant ω (2) for an interface between vacuum ($z<0$) and LHM ($z>0$). LHM is described by Eq. (8) with the following parameters: $\omega_{rm2}=0$, $\omega_{pe2}=\omega_{pm2}=2\pi 15\times 10^9$ s^{-1}, and $\omega_{de2}=\omega_{dm2}=10^{-3}\omega_{pe2}$; $q=-1$ nC, $R=9.5$ cm ($R<\rho_2^*\cot\theta_{10}^*$ for all used parameters). Frequencies indicated on plots are in units of ω_{pe2}.

should be noted that parameters R_1^* and ρ_2^* determining areas of the RCTR and CR significance can be relatively large for the interface with real metamaterials. For example, the dependence of R_1^* in units of $c\omega^{-1}$ on charge velocity β for $n_1=1$, $n_2=-1.5+i0.01$ (see Refs. 50 and 51) is presented in Fig. 5. As one can see, RCTR on GHz frequencies penetrates vacuum a distance around several meters, which is more than sufficient for registration. In the lossless case [Fig. 4(a)] reflected RCTR exists outside the cone $\pi/2<\theta<\pi-\theta_{20}^*$, refracted RCTR exists in the whole half-space $z<0$. Besides, in both cases RCTR is concentrated near the charge motion line due to the negative refraction at the interface (see the interference areas of refracted RCTR in Fig. 4). The obtained uniform asymptotic approximations (A1) ($z<0$) and a similar expression for $z>0$ correctly describe the field behavior within the half-shadow areas, i.e., the vicinities of the refracted and reflected CR angles: $|\theta-\theta_1^*|\lesssim\Delta\theta_1$ and $|\theta-\theta_2^*|\lesssim\Delta\theta_2$, respectively. TR (treated as the saddle-point contribution) is a simple spherical wave outside these areas only. In the lossless case the half-shadow areas exist at arbitrary large distance R, while in the lossy case they are bounded.

B. Numerical approach

Here, we present an effective algorithm for computation of integrals in Eqs. (15) and (16). In contrast to RHFB situation [Fig. 3(Ia)], in the LHFB case, poles $\pm s_2$ are located near the integration path [Fig. 3(IIa)]. This leads to rather abrupt behavior of integrands in Eq. (16). Our numerical algorithm is adapted for overcoming this difficulty by means of appropriate choosing the integration step in the poles' vicinities. It is noteworthy that numerical and analytical methods are in a good agreement in the domain of the asymptotic validity of the latter. Below the most significant results of numerical calculation are presented.

To illustrate the main effects, we suppose that medium 1 is vacuum and medium 2 is described by the dielectric and

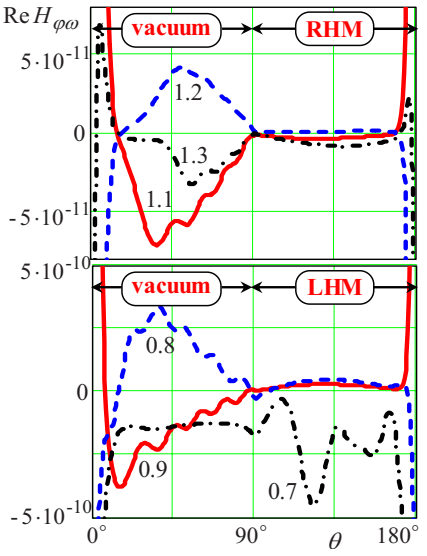

FIG. 9. (Color online) Dependence of the magnetic field Fourier harmonic Re $H_{\varphi\omega}$ (Vm^{-1} s) on the angle θ for the situation where Cherenkov condition is not fulfilled, $\beta<\beta_{CR}$. The top plot corresponds to the frequencies inside RHFB (vacuum-RHM transition), the bottom plot corresponds to the frequencies inside LHFB (vacuum-LHM transition). Frequencies (in units of ω_{pe2}) are indicated near the curves. Medium 2 is described by Eq. (8) with the parameters same as in Fig. 8.

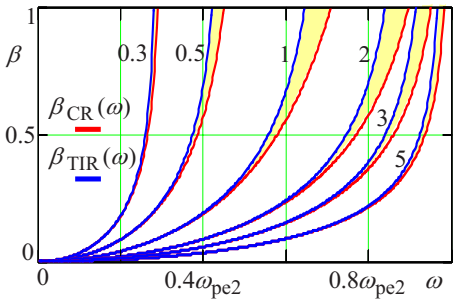

FIG. 10. (Color online) Modification of the RCTR effect area [the region enclosed between $\beta_{CR}(\omega)$ and $\beta_{TIR}(\omega)$] with the increase in the ratio $\omega_{pm2}/\omega_{pe2}$. This ratio is indicated near each area.

magnetic constants in Eq. (8) with $\omega_{rm}=0$ ($\omega_{de} \ll \omega_{pe}$, $\omega_{dm} \ll \omega_{pm}$). Moreover, unless otherwise specified, we suppose the electric and magnetic plasma frequencies be equal to each other: $\omega_{pe2}=\omega_{pm2}$. The dependences of n_2^2, ε_2, and μ_2 on ω in the lossless case ($\omega_{de2}=\omega_{dm2}=0$) are presented in Fig. 6. As one can see, medium 2 have both RHFB ($\omega > \omega_{pe2}$) and LHFB ($0 < \omega < \omega_{pe2}$).

Recall that RCTR in vacuum is generated provided that condition (31) is fulfilled. The dependence of β_{CR} and β_{TIR} on frequency is presented in Fig. 7.

The allowable parameters (β, ω) for vacuum RCTR effect are those enclosed between β_{CR} and β_{TIR} (Fig. 7). Thus we have at least two possibilities to demonstrate the RCTR effect: to vary frequency ω at constant β (path 1 in Fig. 7) or to vary velocity β at constant ω (path 2 in Fig. 7). In the first case RCTR exists within the frequency range $\omega_c^- < \omega < \omega_c^+$, where $\omega_c^- = \omega_{pe2}\sqrt{\beta[\beta+\sqrt{1+\beta^2}]^{-1}}$, $\omega_c^+ = \omega_{pe2}\sqrt{\beta[1+\beta]^{-1}}$ (losses are neglected). In the second case RCTR exists within the range of velocities $\beta_{CR} < \beta < \beta_{TIR}$.

To demonstrate the effect we consider the spatial distribution of the Fourier harmonic of the magnetic field $H_{\varphi\omega}$ [see Eq. (16)], i.e., the dependence of Re $H_{\varphi\omega}$ on angle θ at constant R (see semicircle in Fig. 2). The modification of this dependence with the increase in ω or β along paths 1 and 2, correspondingly, (Fig. 7) is presented in Fig. 8. For observing the interference in the refracted RCTR the distance R was chosen to satisfy the condition $R < \rho_2^* \cot \theta_{10}^*$ [see Fig. 4(b)].

Figure 8 confirms that RCTR in vacuum is the double-threshold effect in both frequency and velocity domain, in

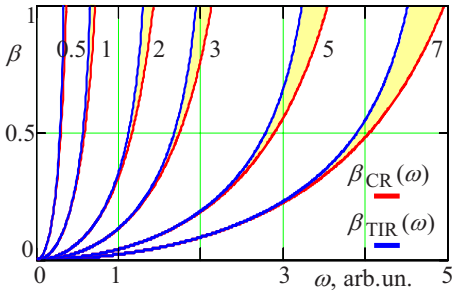

FIG. 11. (Color online) Modification of the RCTR effect area [the region enclosed between $\beta_{CR}(\omega)$ and $\beta_{TIR}(\omega)$] with the increase in the magnitude of $\omega_{pe2}=\omega_{pm2}$. This value (in arbitrary units) is indicated near each area.

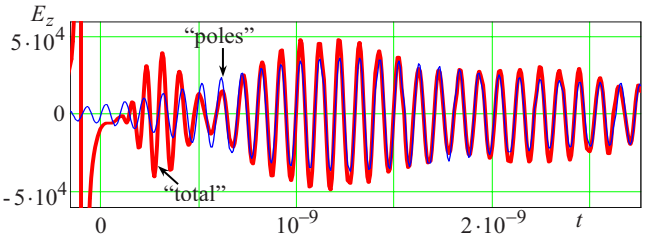

FIG. 12. (Color online) The time dependence of E_z component (V/m) at fixed spatial point in vacuum: $z=-3.2$ cm and $\rho=0.03$ cm; medium 2 is described by Eq. (8) with the following parameters: $\omega_{rm2}=0$, $\omega_{pe2}=\omega_{pm2}=2\pi 10\times 10^9$ s^{-1}, and $\omega_{de2}=\omega_{dm2}=10^{-4}\omega_{pe2}$; $\beta=0.99$, $\omega_c^-=0.64\omega_{pe2}$, and $\omega_c^+=0.71\omega_{pe2}$.

accordance with Eq. (31) and Fig. 7. Moreover, formula (26) predicts that contributions of poles $\pm\psi_2$ may interfere at angles $\theta < \theta_1^*$, where both of them exist. This interference in Fig. 8 is evident at angles $\theta < 45°$ for $\beta=0.8$ and $\omega=0.63$–$0.64\omega_{pe2}$. Interference of the pole s_2 contribution with the forced field (4) is visible in Fig. 8 at angles $90° < \theta < 135°$ for $\omega=0.63\omega_{pe2}$, $\beta=0.9$–0.95 and for $\omega=0.6\omega_{pe2}$, $\beta=0.8$.

The aforementioned peculiarities of the spatial radiation in the present geometry are explained by the reversed nature of CR in LHM and by the unusual law of refraction at RHM-LHM interface (Fig. 4). The RCTR in RHM (refracted CR) consists of waves propagating both toward and away from the z axis. They interfere inside the cone determined by the refracted CR angle θ_1^*. In LHM the reflected waves of RCTR interfere with reversed CR outside the cone determined by the reflected CR angle θ_2^*.

It is of interest to discuss separately the main features of TR. For this purpose we will consider the situation where $\beta < \beta_{CR}$, both CR and RCTR are absent, and the only spatial radiation one would expect here is TR. The dependence of the magnetic field Fourier harmonic Re $H_{\varphi\omega}$ on θ at $R=$const (dashed half-circle in Fig. 2) for this situation is presented in Fig. 9. The top plot of Fig. 9 corresponds to the frequencies from RHFB ($\omega > \omega_{pe2}$) while the bottom one corresponds to the frequencies from LHFB ($\omega_c^+ < \omega < \omega_{pe2}$). First, TR is about 1–2 order smaller as compared with CR and RCTR for given parameters. Second, one can see that in the bottom case (vacuum-LHM transition), the TR in vacuum is much larger as compared with the top case (vacuum-RHM transition). Thus, TR is generated more effectively in the case of vacuum-LHM interface.

To discuss the possible applications of the vacuum RCTR effect we will show how the area of this effect [in (β, ω) space] is affected by the parameters of medium 2. The modification of the vacuum RCTR effect area under changes in ratio $\omega_{pm2}/\omega_{pe2}$ and the absolute value of ω_{pe2} is presented in Figs. 10 and 11, respectively. As one can see, the width of this area is nonmonotonic function of $\omega_{pm2}/\omega_{pe2}$ while at fixed ratio (the case $\omega_{pm2}=\omega_{pe2}$ is presented in Fig. 11) this width increases monotonously with increasing absolute values of ω_{pe2} and ω_{pm2}.

The aforementioned peculiarities can be applied to both diagnostics of beams and characterization of LHM. First, the double threshold detector can be designed to separate par-

ticles with velocities within the predetermined range. Choosing the proper MTM and fixing the frequency of registration, the desired lower and upper thresholds can be attained. Moreover, measuring the RCTR spectra produced by monoenergetic beams with known energy, the experimental area of the RCTR effect (similar to Fig. 7) can be obtained and the appropriate effective parameters (ε,μ) can be chosen to give a good fit to observed data.

Further, we will demonstrate how the RCTR effect manifests itself in the total field. Figure 12 presents the time dependence of E_z component of the total field (14) at the fixed point in the area $z<0$ (vacuum). Figure 12 demonstrates that RCTR can be the dominant radiation. The bold-face line in Fig. 12 corresponds to the total field (14) while the light-face line represents the result of integration of the poles' contribution (26) (determining RCTR) over frequency. One can see that for $t>0.7\times10^{-9}$ s, the total field is very well approximated by the contribution of the poles. Therefore, in this case, RCTR gives the main contribution to the spatial radiation. For $t<0.7\times10^{-9}$ s the dominant radiation is TR. It is noteworthy that the TR and RCTR fields are separated by considerable time delay, allowing their independent registration.

IV. CONCLUSION

We have analyzed the electromagnetic field of a uniformly moving point charge in two cases. The first case is in unbounded LHM. Using methods developed in our previous publications, we have presented the electromagnetic field as a sum of three physically different summands having clear physical meaning: quasi-Coulomb field, wave field (Cherenkov radiation) and plasma trace. Additionally, we have developed an effective algorithm for numerical calculation of the total field and presented a number of typical field plots and energetic patterns of radiation. It has been demonstrated that wave field in LHM lags behind the charge more so than it does in the RHM case. As a result, if a medium supports both left-handed and right-handed CR, a considerable time delay exists between the corresponding field peaks. The latter fact can be useful for the experimental registration of CR in MTMs and for the MTM diagnostics.

The second geometry is a plane boundary between ordinary medium and LHM intersected transversely by the charge. The asymptotic approximations for the Fourier harmonics of the field have been obtained and the effective algorithm for the computation of both total field and it's Fourier harmonics have been developed. As it has been shown, three types of spatial radiation can exist in this case: transition radiation, Cherenkov radiation, and RCTR. The case of a vacuumlike medium bordering a left-handed metamaterial has been investigated in more detail. Rigorous conditions for generating RCTR have been obtained: RCTR in the vacuum area is a double threshold effect in both frequency and charge velocity domain. The dependencies of these thresholds on parameters of LHM have been investigated. The RCTR decay in vacuum due to the losses in LHM has been studied and areas of the RCTR significance have been determined.

As was shown, RCTR can penetrate vacuum a distance sufficiently large for observation. It has been demonstrated that TR is generated more effectively at the vacuum-LHM interface as compared with the vacuum-RHM interface. Besides, we have determined the half-shadow areas, i.e., areas where TR is not a simple spherical wave and cannot be described separately from RCTR and CR. These areas are narrow regions near the reflected and refracted CR angles. They exist at arbitrary large distance in the lossless case and have a finite size in the lossy one. Typical plot of the total magnetic field has been calculated as well. It has been demonstrated that RCTR field can be separated from TR field in the time domain and is the dominant radiation for relatively large time. Possible applications of the vacuum RCTR effect to the beam diagnostics and LHM characterization have been suggested.

ACKNOWLEDGMENTS

The authors would like to thank A. Kanareykin, P. Schoessow, T. Yu. Alekhina, and E. G. Doil'nitsina for useful discussions. This research was supported by the Education Agency of Russian Federation and the Russian Foundation for Basic Research (Grant No. 09-02-00921a).

APPENDIX: UNIFORM ASYMPTOTIC REPRESENTATION IN THE LHFB CASE

When condition (31) is fulfilled, the pole $-\psi_2$ is situated near the saddle point $\psi=\theta$. In this case, asymptotic approximation of the integral along Γ_{SDP} has the form[52]

$$\begin{Bmatrix} E_{\rho\omega}^{\mathrm{b1S}} \\ E_{z\omega}^{\mathrm{b1S}} \\ H_{\varphi\omega}^{\mathrm{b1S}} \end{Bmatrix} \approx \frac{\sqrt{2}\exp(i\kappa_1 R)}{\sqrt{\pi R\sin\theta}} \left[\sqrt{\frac{\pi}{\Omega_1}} \begin{Bmatrix} T_{\rho\omega}^{(1)} \\ T_{z\omega}^{(1)} \\ T_{\varphi\omega}^{(1)} \end{Bmatrix} \pm 2i\sqrt{\pi} \begin{Bmatrix} a_{\rho\omega}^{(1)} \\ a_{z\omega}^{(1)} \\ a_{\varphi\omega}^{(1)} \end{Bmatrix} e^{-\Omega_1 b_1^2} Q(\pm ib_1\sqrt{\Omega_1}) \right], \quad \mathrm{Im}\, b_1 \gtrless 0, \tag{A1}$$

$$\begin{Bmatrix} T_{\rho\omega}^{(1)} \\ T_{z\omega}^{(1)} \\ T_{\varphi\omega}^{(1)} \end{Bmatrix} = h_1 \begin{Bmatrix} e_{\rho\omega}^{\mathrm{b1}}(\theta,\omega) \\ e_{z\omega}^{\mathrm{b1}}(\theta,\omega) \\ h_{\varphi\omega}^{\mathrm{b1}}(\theta,\omega) \end{Bmatrix} + \frac{1}{b_1} \begin{Bmatrix} a_{\rho\omega}^{(1)} \\ a_{z\omega}^{(1)} \\ a_{\varphi\omega}^{(1)} \end{Bmatrix}, \tag{A2}$$

$$\begin{Bmatrix} a_{\rho\omega}^{(1)} \\ a_{z\omega}^{(1)} \\ a_{\varphi\omega}^{(1)} \end{Bmatrix} = \frac{\varepsilon_1}{n_1\sqrt{\pm s_2}} \begin{Bmatrix} \dfrac{\pm\kappa_1 s_2 k_z^1(s_2)}{\omega\varepsilon_1 g_3^*(\omega)} \exp\left(\dfrac{-3\pi i}{4}\right) \\ \dfrac{-i\kappa_1 s_2^2}{\omega\varepsilon_1 g_3^*(\omega)} \exp\left(\dfrac{-\pi i}{4}\right) \\ \dfrac{\mp\kappa_1 s_2}{c g_3^*(\omega)} \exp\left(\dfrac{-3\pi i}{4}\right) \end{Bmatrix}, \tag{A3}$$

where $b_1(\omega)=\sqrt{\phi_1(\theta)-\phi_1(-\psi_2)}$, $\arg b_1$ is defined so that $b_1 \to (-\psi_2-\theta)/h_1$ as $-\psi_2\to\theta$, $Q(y)=\int_y^\infty \exp(-\xi^2)d\xi$, $\mathrm{Re}\sqrt{\pm s_2}>0$, and g_3^* is given by Eq. (30). In this case, the expressions for $E_{\rho\omega}^{\mathrm{b1S}}$, $E_{z\omega}^{\mathrm{b1S}}$, and $H_{\varphi\omega}^{\mathrm{b1S}}$ are more complicated (not simple

spherical waves) and cannot be separated from the poles' contribution because of the discontinuity in Eq. (A1) as $\mathrm{Im}\, b_1$ changes from positive to negative values. One can obtain that $\mathrm{Im}\, b_1=0$ at $\theta=\theta_1^*$, where θ_1^* is expressed by Eq. (28). This discontinuity in each component is exactly equal to corresponding residue in the pole $-\psi_2$ [Eq. (27)].

When $|b_1|\sqrt{\Omega_1}\gg 1$, one can decompose $Q(\pm ib_1\sqrt{\Omega_1})$ into a series. As a result, we obtain Eq. (32) from Eq. (A1).

Supposing Eq. (31) is fulfilled and $\mathrm{Im}\, s_2^2 \ll \mathrm{Re}\, s_2^2$, $\mathrm{Im}[k_z^{(1)}(s_2)]^2 \ll \mathrm{Re}[k_z^{(1)}(s_2)]^2$, one can decompose s_2 and $k_z^{(1)}(s_2)$ into the series

$$s_2 \approx -\frac{\omega}{c\beta}\left[\sqrt{\mathrm{Re}\, n_2^2\beta^2-1}+\frac{i\,\mathrm{Im}\, n_2^2\beta^2}{2\sqrt{\mathrm{Re}\, n_2^2\beta^2-1}}+\frac{(\mathrm{Im}\, n_2^2)^2\beta^4}{8(\mathrm{Re}\, n_2^2\beta^2-1)^{3/2}}\right],$$

$$k_z^{(1)}(s_2) \approx \frac{\omega}{c\beta}\left[\sqrt{n_1^2\beta^2-\mathrm{Re}\, n_2^2\beta^2+1}-\frac{i\,\mathrm{Im}\, n_2^2\beta^2}{2\sqrt{n_1^2\beta^2-\mathrm{Re}\, n_2^2\beta^2+1}}+\frac{(\mathrm{Im}\, n_2^2)^2\beta^4}{8(n_1^2\beta^2-\mathrm{Re}\, n_2^2\beta^2+1)^{3/2}}\right]. \quad \text{(A4)}$$

As a result, it is easy to demonstrate that $|b_1|\sqrt{\Omega_1}$ has a minimum at $\theta=\theta_1^*$

$$|b_1|\sqrt{\Omega_1}|_{\min} \approx \sqrt{R/R_1^*}, \quad \text{(A5)}$$

where the expression for θ_1^* and R_1^* are given by Eqs. (28) and (29), respectively. Note that $R_1^*\kappa_1 \gg 1$ based on the above assumptions concerning the relation between real and imaginary parts of s_2 and $k_z^{(1)}(s_2)$. For $R\gg R_1^*$, the condition $|b_1|\sqrt{\Omega_1}\gg 1$ is fulfilled at an arbitrary angle within the range $1/\sqrt{\Omega_1}\ll\theta<\pi/2$ and Eq. (33) is true. Furthermore, one can obtain that $|b_1|\sqrt{\Omega_1}\lesssim 1$ inside the angular interval $|\theta-\theta_1^*| \lesssim \Delta\theta_1$, where $\Delta\theta_1=\sqrt{2\Omega_1^{-1}(1-R/R_1^*)}$.

Losses in medium 2 result in exponential decay of the poles' contribution (26)

$$\begin{Bmatrix} |E_{\rho\omega}^{\mathrm{b1P}\pm}| \\ |E_{z\omega}^{\mathrm{b1P}\pm}| \\ |H_{\varphi\omega}^{\mathrm{b1P}\pm}| \end{Bmatrix} \sim \exp\left[-\frac{2R}{R_{1\pm}^*(\theta)}\right], \quad \text{(A6)}$$

where

$$R_{1\pm}^* = \frac{4n_1\sin\theta_{10}^*\cos\theta_{10}^*}{\omega\beta|\mathrm{Im}\, n_2^2|\sin(\theta_{10}^*\pm\theta)} \quad \text{(A7)}$$

and θ_{10}^* is determined by Eq. (28). The least decay is exhibited by the contribution of pole $-\psi_2$ at $\theta=\theta_1^*$: $R_{1-}^*(\theta_1^*)=R_1^*$ and we arrive at Eq. (34). Consequently, R_1^* determines the area where the poles' contribution (26) and the uniform asymptotic (A1) (in the vicinity of θ_1^*) should be taken into account.

*galiaminsn@yandex.ru
†tyukhtin@bk.ru

[1] V. G. Veselago, Sov. Phys. Usp. **10**, 509 (1968).
[2] V. G. Veselago, Phys. Usp. **46**, 764 (2003).
[3] L. I. Mandel'shtam, Zh. Eksp. Teor. Fiz. **15**, 475 (1945).
[4] L. I. Mandel'shtam, *Lectures on Optics, the Theory of Relativity, and Quantum Mechanics* (Moskow University Press, Moscow, 1972).
[5] A. Moroz, http://www.wave-scattering.com/negative.html
[6] V. M. Agranovich and Y. N. Gartstein, in *Physics of Negative Refraction and Negative Index Materials*, Springer Series in Materials Science, edited by K. M. Krowne and Y. Zhang (Springer-Verlag, New York, 2007), Vol. 98, pp. 95–132.
[7] J. B. Pendry, A. J. Holden, W. J. Stewart, and I. Youngs, Phys. Rev. Lett. **76**, 4773 (1996).
[8] J. B. Pendry, A. J. Holden, D. J. Robins, and W. J. Stewart, IEEE Trans. Microwave Theory Tech. **47**, 2075 (1999).
[9] D. R. Smith, W. J. Padilla, D. C. Vier, S. C. Nemat-Nasser, and S. Schultz, Phys. Rev. Lett. **84**, 4184 (2000).
[10] R. W. Ziolkowsky, IEEE Trans. Antennas Propag. **51**, 1516 (2003).
[11] R. A. Shelby, D. R. Smith, S. C. Nemat-Nasser, and S. Schultz, Appl. Phys. Lett. **78**, 489 (2001).
[12] T. J. Yen, W. J. Padilla, N. Fang, D. C. Vier, D. R. Smith, J. B. Pendry, D. N. Basov, and X. Zhang, Science **303**, 1494 (2004).
[13] S. Linden, C. Enkrich, M. Wegener, J. Zhou, T. Koschny, and C. M. Soukoulis, Science **306**, 1351 (2004).
[14] H. O. Moser, B. D. F. Casse, O. Wilhelmi, and B. T. Saw, Phys. Rev. Lett. **94**, 063901 (2005).
[15] C. M. Soukoulis, J. Zhou, T. Koschny, M. Kafesaki, and E. N. Economou, J. Phys.: Condens. Matter **20**, 304217 (2008).
[16] A. Pimenov, A. Loidl, K. Gehrke, V. Moshnyaga, and K. Samwer, Phys. Rev. Lett. **98**, 197401 (2007).
[17] D. R. Smith and N. Kroll, Phys. Rev. Lett. **85**, 2933 (2000).
[18] R. W. Ziolkowski and E. Heyman, Phys. Rev. E **64**, 056625 (2001).
[19] S. Foteinopoulou, E. N. Economou, and C. M. Soukoulis, Phys. Rev. Lett. **90**, 107402 (2003).
[20] J. Pacheco, T. M. Grzegorczyk, B.-I. Wu, Y. Zhang, and J. A. Kong, Phys. Rev. Lett. **89**, 257401 (2002).
[21] T. Koschny, M. Kafesaki, E. N. Economou, and C. M. Soukoulis, Phys. Rev. Lett. **93**, 107402 (2004).
[22] D. R. Smith, D. C. Vier, T. Koschny, and C. M. Soukoulis, Phys. Rev. E **71**, 036617 (2005).
[23] D. R. Smith, Phys. Rev. E **81**, 036605 (2010).
[24] J. Lu, T. M. Grzegorczyk, Y. Zhang, J. P. Jr, B. I. Wu, and J. A. Kong, Opt. Express **11**, 723 (2003).
[25] Z. Y. Duan, B.-I. Wu, S. Xi, H. S. Chen, and M. Chen, Prog. Electromagn. Res. **90**, 75 (2009).
[26] Y. O. Averkov, A. V. Kats, and V. M. Yakovenko, Phys. Rev. B **79**, 193402 (2009).
[27] B.-I. Wu, J. Lu, and J. A. Kong, J. Appl. Phys. **102**, 114907 (2007).
[28] S. Xi, H. Chen, T. Jiang, L. Ran, J. Huangfu, B.-I. Wu, J. A.

Kong, and M. Chen, Phys. Rev. Lett. **103**, 194801 (2009).
[29] V. E. Pafomov, Sov. Phys. JETP **9**, 1321 (1959).
[30] Y. O. Averkov, Telecommun. Radio Eng. **63**, 419 (2005).
[31] A. V. Tyukhtin, Tech. Phys. Lett. **31**, 150 (2005).
[32] A. D. Kanareykin and A. V. Tyukhtin, Nucl. Instrum. Methods Phys. Res. A **558**, 62 (2006).
[33] N. V. Ivanov and A. V. Tyukhtin, Tech. Phys. Lett. **32**, 449 (2006).
[34] A. V. Tyukhtin, A. Kanareykin, and P. Schoessow, Phys. Rev. ST Accel. Beams **10**, 051302 (2007).
[35] S. N. Galyamin and A. V. Tyukhtin, Vestn. St. Petersburg Univ., Ser. 4: Fiz., Khim. **1**, 21 (2006) in Russian.
[36] A. V. Tyukhtin and S. N. Galyamin, Tech. Phys. Lett. **33**, 632 (2007).
[37] A. V. Tyukhtin and S. N. Galyamin, Phys. Rev. E **77**, 066606 (2008).
[38] S. N. Galyamin, A. V. Tyukhtin, A. Kanareykin, and P. Schoessow, Phys. Rev. Lett. **103**, 194802 (2009).
[39] I. E. Tamm and I. M. Frank, C. R. Acad. Sci. URSS **14**, 107 (1937).
[40] I. M. Frank, *Vavilov-Cherenkov Radiation: Theoretical Aspects* (Nauka, Moscow, 1988) in Russian.
[41] V. P. Zrelov, *Vavilov-Cherenkov Radiation in High-Energy Physics* (Israel Program for Scientific Translations, Jerusalem, 1970).
[42] E. Fermi, Phys. Rev. **57**, 485 (1940).
[43] V. L. Ginzburg and I. M. Frank, Zh. Eksp. Teor. Fiz. **16**, 15 (1946).
[44] V. L. Ginzburg and V. N. Tsytovich, *Transition Radiation and Transition Scattering* (Hilger, London, 1990).
[45] B. M. Bolotovskiy and S. N. Stolyarov, in *Problems of Theoretical Physics: Collection of I. E.Tamm's Memory* (Nauka, Moscow, 1972), p. 267.
[46] G. M. Garibian, Sov. Phys. JETP **6**, 1079 (1958).
[47] E. A. Kaner and V. M. Yakovenko, Sov. Phys. JETP **15**, 330 (1962).
[48] F. G. Bass and V. M. Yakovenko, Sov. Phys. Usp. **8**, 420 (1965).
[49] L. M. Brekhovskih, *Waves in Layered Media* (Academic Press, New York, 1980).
[50] P. Markoš, I. Rousochatzakis, and C. M. Soukoulis, Phys. Rev. E **66**, 045601(R) (2002).
[51] J.-F. Wang, S.-B. Qu, Z. Xu, J.-Q. Zhang, H. Ma, Y.-M. Yang, and C. Gu, Chin. Phys. Lett. **26**, 084103 (2009).
[52] L. B. Felsen and N. Marcuvitz, *Radiation and Scattering of Waves* (Wiley Interscience, New Jersey, 2003).